

Journal of Fire Sciences

<http://jfs.sagepub.com>

Enclosure Fires, Gravity Waves, and the Backdraft Problem

Jónas Eliasson, Georges Guigay and Bjorn Karlsson

Journal of Fire Sciences 2008; 26; 373

DOI: 10.1177/0734904108092116

The online version of this article can be found at:
<http://jfs.sagepub.com/cgi/content/abstract/26/5/373>

Published by:



<http://www.sagepublications.com>

Additional services and information for *Journal of Fire Sciences* can be found at:

Email Alerts: <http://jfs.sagepub.com/cgi/alerts>

Subscriptions: <http://jfs.sagepub.com/subscriptions>

Reprints: <http://www.sagepub.com/journalsReprints.nav>

Permissions: <http://www.sagepub.co.uk/journalsPermissions.nav>

Citations <http://jfs.sagepub.com/cgi/content/refs/26/5/373>

Enclosure Fires, Gravity Waves, and the Backdraft Problem

JÓNAS ELÍASSON AND GEORGES GUIGAY*

*Department of Civil and Environmental Engineering, University of Iceland
Sudurgata, 108 Reykjavík, Iceland*

BJORN KARLSSON

Iceland Fire Authority, Skúlagötu 21, 101 Reykjavík, Iceland

(Received May 16, 2006)

ABSTRACT: The air flow to an underventilated compartment fire often depends on the flow velocities in the gravity wave of cold air that feeds the fire with oxygen. This problem has been studied in laboratory experiments and by CFD simulations. The main problem seems to be whether mixing and entrainment between the two layers of hot and cold air has a profound effect on the flow velocities. In this article, an analytical gravity wave model that can calculate the velocities in a simple gravity wave is presented. This model uses the equations of stratified flow hydraulics and the translatory wave solution of the flow equations. It is found that the velocities of the model compare very well to the velocities reported from laboratory tests and numerical simulations. Numerical simulations of stratified flow in a CFD model are discussed with respect to model construction. It is concluded that the densimetric Froude number is the main parameter for the velocity calculations and the length/height ratio is important for the friction forces.

KEY WORDS: backdraft, gravity wave, density driven flow.

INTRODUCTION

UNTIL RECENTLY, LITTLE research had been done on backdraft [1–4] in spite of how dangerous this phenomenon is to firefighters. This event is

*Author to whom correspondence should be addressed. E-mail: gig3@hi.is
Figure 4 appears in color online: <http://jfs.sagepub.com>

very hazardous and dangerous and has killed many firefighters in the past years [5]. The reason is undoubtedly the great difficulty in understanding this complicated process: first the accumulation of gases from an underventilated flame, then the gravity wave that carries oxygen into the compartment, and finally the ignition and the backdraft explosion itself. When an underventilated fire dies from a lack of oxygen, the enclosed room can remain full of hot unburned gases. If firefighters enter through a door, a window breaks or an opening occurs, fresh oxygen is carried in by gravity currents, and mixes with the gases. The crucial element is this wavelike gravity current, i.e., whether its dilution with gases and smoke into a flammable mixture results in backdraft or not.

The single most difficult detail in backdraft study is undoubtedly the time that elapses from the opening of the compartment until the occurrence of the explosion, which is the time it takes for the gravity wave to roll in and create the explosive mixture. This problem is highly fluid mechanical in character and is therefore best studied by the classical methods of fluid mechanics, reduced scale experiments [1–3,6–8], CFD numerical modeling [9,10], and mathematical analysis. Successful backdraft mitigation demands an understanding of the gravity wave.

This study focuses on the velocity and thickness of the gravity wave that causes backdraft. Stratified fluid dynamics are applied to find the thickness (height) and the velocity of the gravity wave that carries fresh air into the compartment. The travel time of the wave from the opening to the point of possible ignition and the oxygen carrying capacity of the wave may thus be estimated. To do this, the translatory wave theory is used [11], originally developed by Stoker [12], and adapted to stratified flow using [13], which is a very complete and detailed work on gravity waves, describing in detail the theory of non-miscible and miscible stratified flow, as well as wind-driven and buoyant flow. The fluid mechanical part of the analysis is enclosed in the Appendix and will be referred to as necessary.

GRAVITY WAVE ON A FLAT BOTTOM

A gravity wave is studied here, which progresses at a velocity V (see Figures 1 and 2). At first the compartment is closed, but then suddenly a wall opens. Cold air flows in and an equal amount of hot air flows out.

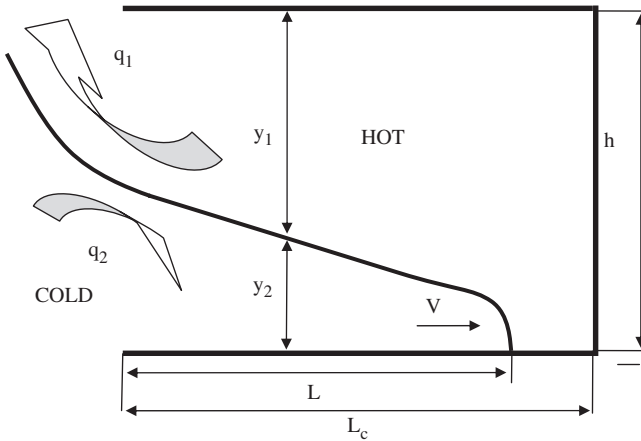


Figure 1. Definition sketch of a gravity wave flowing through a full opening.

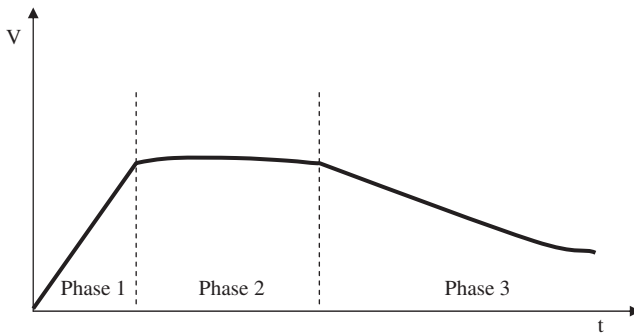


Figure 2. Time history of the flow entering a flat bottom compartment.

When the door opens, the initial pressure surge will settle down quickly and a neutral plane will develop near the middle of the opening, with inflowing air below and outflowing air above. The gravity wave will then develop in three phases, provided the compartment is long enough. A time history of the flow will look like as shown in Figure 2.

One can see that the evolution of the flow can be divided into three different phases. During Phase 1, the wave accelerates from zero to full velocity. The second phase is the translatory wave, moving with almost constant velocity (see Stoker's theory described in [12]). Finally, the third phase is the retarding wave, when it loses momentum and slows down.

Phase 1: The Accelerating Phase

Just after the opening is lifted, the flow velocities are small, the friction negligible, and one can use the unsteady Bernoulli equation.

$$\frac{\partial}{\partial t} \rho \phi + P + \rho g z + \frac{1}{2} \rho V^2 = Cst. \quad (1)$$

Taking the gradient of this equation, one obtains:

$$\frac{\partial}{\partial t} (\rho \vec{\nabla} \phi) + \vec{\nabla} \left(P + \rho g z + \frac{1}{2} \rho V^2 \right) = 0. \quad (2)$$

Multiplying by $\overline{dS} = (\overline{dx} \cdot \overline{dy})$ and integrating along a closed curve that is a fluid pathline, one gets:

$$\frac{\partial}{\partial t} \oint \rho (V_x dx + V_y dy) = \frac{\partial}{\partial t} \oint |V| dS \quad (3)$$

$$\frac{\partial}{\partial t} \oint |V| dS + \oint d \left(P + \rho g z + \frac{1}{2} \rho V^2 \right) = 0 \quad (4)$$

or

$$\rho_2 \frac{\partial}{\partial t} \overline{V} \ell = \Delta \rho_2 g h (\overline{V}: \text{average velocity over } \ell). \quad (5)$$

If one lets the pathline touch the floor and the surface, with $\ell \approx (L + h)$, $\partial \overline{V} / \partial t$ will be nearly constant until $L \approx h$.

In an accelerating translatory wave, one will have:

$$\rho_2 \frac{DV}{Dt} = \rho_2 \frac{\partial V}{\partial t} \text{ as } \frac{\partial V}{\partial x} \approx 0. \quad (6)$$

$\partial V / \partial t$ is higher in the wave than elsewhere on a closed path line and proportional to the average acceleration. Now, by using the proportionality factor obtained from the unsteady Bernoulli equation and including the acceleration forces in the depth integrated energy equation for the gravity wave as an unknown inertial force, one gets:

$$\rho_2 \frac{\partial V}{\partial t} y_2 = -\Delta \rho_2 g \frac{\partial y_2}{\partial x} y_2 - \tau \quad (7)$$

where τ is the combined interfacial and bottom shear stress. Equation (7) shows how the acceleration term on the left hand side is

balanced by the pressure gradient in Phase 1 if the friction τ is almost zero. Later, in Phase 2, the acceleration term becomes zero and shear stress and pressure gradient will balance each other. When the acceleration term becomes zero, Equation (2) turns into the Bernoulli equation. It will approximately hold for the flow outside the box in the cold fluid as velocities are low here. This gives an estimate of the maximum velocity of the flow into the box. A neutral plane at $y = h/2$ is estimated. Applying Bernoulli's equation to a streamline, close to the bottom, one obtains:

$$V = \sqrt{\Delta gh} \quad \text{with } \Delta = \frac{\rho_2 - \rho_1}{\rho_2}. \quad (8)$$

Assuming linear acceleration (no friction) as shown in Figure 2, the average velocity is:

$$V_{\text{av}} = \frac{1}{2} V_{\text{max}}. \quad (9)$$

Equation (5) can be used to estimate roughly the time necessary to accelerate the fluid up to the Bernoulli velocity. One gets:

$$t_a = \ell / \sqrt{\Delta gh}. \quad (10)$$

Phase 2: The Translatory Phase

In air, only confined (closed) flow is possible, but in mixing zones of salt and fresh water, unconfined (free surface) flow is the rule. With hydrostatic pressure distribution everywhere in the compartment one would have:

$$\rho_1 h = \rho_1 y_1 + \rho_2 y_2. \quad (11)$$

It is easy to see that the pressure gradient alongside the bottom is zero for this pressure distribution, and therefore no fluid would flow into the compartment. This is the case when dealing with stationary salt water wedges, that can be regarded as translatory waves with zero wave velocity. Behind the salt water wedge where $y_2 = 0$, one has $y_1 = (1 + \Delta)h$, so fluid will be flowing out under the action of a pressure head Δh . This extra fluid depth behind the wedge does not exist in confined flows, where $y_1 + y_2 = h$ always holds. But by using Boussinesq's approximation, one can exclude Δ everywhere except in pressure gradient (buoyancy) terms, and then proceed to treat confined and unconfined flow the same way.

It is noted that the dense bottom current is treated as an open channel flow in a gravity field Δg instead of g . Equations (A1)–(A7) in Appendix 1 are for stationary flow, but the open channel flow equations have another solution, a translatory wave with constant wave velocity equal to the water velocity [12]. In this phase, one has a translatory wave pushing the light fluid out, and slowly pushing the interface upwards.

Derivation of the Basic Equation

The continuity equation for the lower flow (see Appendix 1) will be:

$$\frac{\partial q_2}{\partial x} + \frac{\partial y_2}{\partial t} = 0 \Rightarrow \frac{\partial q_2}{\partial x} - V_2 \frac{\partial y_2}{\partial x} = 0. \quad (12)$$

The similar continuity equation for the upper flow gives directly:

$$q_2 = V_2 y_2 = q_1 \Rightarrow V_2 = V_1 \frac{y_1}{y_2}. \quad (13)$$

By definition, the effect of mixing and entrainment on the overall densities will be small in this phase and will thus be disregarded. One can use three equations to analyze the flow:

- The depth integrated energy equation for the upper layer (Equation (A6)).
- The momentum equation for both layers.
- The momentum equation for the lower layer.

(a) The depth integrated energy equation for the upper layer.

$$I = -\frac{d}{dx} \left[y_2 + y_1 + \frac{V_1^2}{2g} \right]. \quad (14)$$

To evaluate the headloss term I , Equation (A7) is used with ρ as the reference density ρ_R , and then one gets:

$$\tau_i = \rho g y_1 I = \frac{f_i}{2} \rho (V_1 + V_2)^2 = \frac{f_1}{2} \rho V_2^2 \left(\frac{h}{y_1} \right)^2. \quad (15)$$

Equation (15) is derived from the more general Equation (A5) by using Boussinesq's approximation mentioned earlier.

By identification between Equations (14) and (15), one obtains:

$$\left[y_2 + y_1 + \frac{V_1^2}{2g} \right]_0^L = \frac{f_i}{2g} V_2^2 \int_0^L \frac{h^2}{y_1^3} dx. \tag{16}$$

Assuming that y_2 is a parabola, it has the equation:

$$\frac{y_2}{h} = \frac{y_{2,0}}{h} \sqrt{1 - \frac{x}{L}} = \psi \sqrt{1 - \frac{x}{L}}. \tag{17}$$

The integral in Equation (16) is solved as:

$$\int_0^L \frac{h^2}{y_1^3} dx = \frac{1}{h} \int_0^L \frac{dx}{(1 - (y_2/h))^3} = \frac{1}{h} \int_0^L \frac{dx}{(1 - \psi \sqrt{1 - (x/L)})^3} = \frac{1}{h(1 - \psi)^2}. \tag{18}$$

Substituting this result in Equation (16), one obtains:

$$y_L - y_{2,0} - y_{1,0} = \frac{V_2^2}{2g} \left(\frac{\psi}{1 - \psi} \right)^2 + \frac{f_i L}{2g h} \frac{V_2^2}{(1 - \psi)^2}. \tag{19}$$

(b) The momentum equation for both layers. This equation results in:

$$y_L - y_{2,0} - y_{1,0} = \frac{1}{2} \Delta h \Psi^2 + \frac{V_2^2}{2g} \frac{2\psi}{1 - \psi} - C_f \frac{V_2^2 L}{g h}. \tag{20}$$

Combining one gets:

$$\frac{V_2}{\sqrt{\Delta g h}} = C_\Delta = \sqrt{\frac{\psi^2}{(\psi/1 - \psi)^2 - (2\psi/1 - \psi) + (L/h)(f_i/(1 - \psi)^2 + 2C_f)}}. \tag{21}$$

(c) The momentum equation for the lower layer. This equation results in:

$$\begin{aligned} & (\Delta h - y_L + y_{2,0} + y_{1,0}) \frac{1}{2} \psi^2 g \rho_2 h \\ &= \int_0^L (\tau_i + \tau) dx = \frac{f_i}{2} \rho_2 V_2^2 L \frac{2}{\psi^2} \left(\frac{\psi}{1 - \psi} + \ln(1 - \psi) \right) + C_f \rho_2 V_2^2 L \end{aligned}$$

or

$$y_L - y_{2,0} - y_{1,0} = \Delta h - \frac{V_2^2 L}{g h} \frac{1}{\psi^2} \left(\frac{2f_i}{\psi^2} \left(\frac{\psi}{1 - \psi} + \ln(1 - \psi) \right) + 2C_f \right). \tag{22}$$

These are equations for V_2 , Y_2 , and Y_L . Then f_i and C_f have to be estimated. Pedersen ([13], Figure 7.2) suggests for f_i :

$$\sqrt{\frac{2}{f_i}} = 2.45 \left(\ln \left(R_{e,i} \sqrt{\frac{f_i}{2}} \right) - 1.3 \right) \quad \text{with } R_{e,i} = \frac{(U_m - U_i)(y - y_0)}{\nu}. \quad (23)$$

The theory for the growing boundary layer can be used to estimate C_f . According to Prandtl (chapter 7 in [14] R_{eL} based on boundary layer length), one has:

$$C_f = \frac{1.310}{R_{eL}^{1/2}} \quad (24)$$

Graphical Method to Find C_A in the Phase 2 Equations

The set of Equations (19), (20), and (22) need to be solved in order to determine C_Δ and ψ knowing the friction coefficients f_i or C_f or vice versa. The following dimensionless coefficients A and B are considered, which represents the frictional effect:

$$A = \frac{L}{h} f_i \quad \text{and} \quad B = 2 \frac{L}{h} C_f. \quad (25)$$

With these coefficients, Equation (21) reduces to:

$$\frac{V_2}{\sqrt{\Delta g h}} = C_{a,\Delta} = \sqrt{\frac{\psi^2}{(\psi/(1-\psi))^2 - (2\psi/(1-\psi)) + A/(1-\psi)^2 + B}}. \quad (26)$$

Combining Equations (20) and (22), one obtains:

$$\begin{aligned} \frac{V_2}{\sqrt{\Delta g h}} &= C_{b,\Delta} \\ &= \sqrt{\frac{\psi^2 - 2}{2(A(1 - (2/\psi^4))(\psi/(1-\psi)) + \ln(1-\psi)) - (B/\psi^2) - (\psi/(1-\psi))}} \end{aligned} \quad (27)$$

This set of equations has to satisfy the condition $C_{a,\Delta} = C_{b,\Delta}$.

This equation set is solved by iteration and used to produce Figure 3. It can be used to find the velocity and the neutral plane height in the

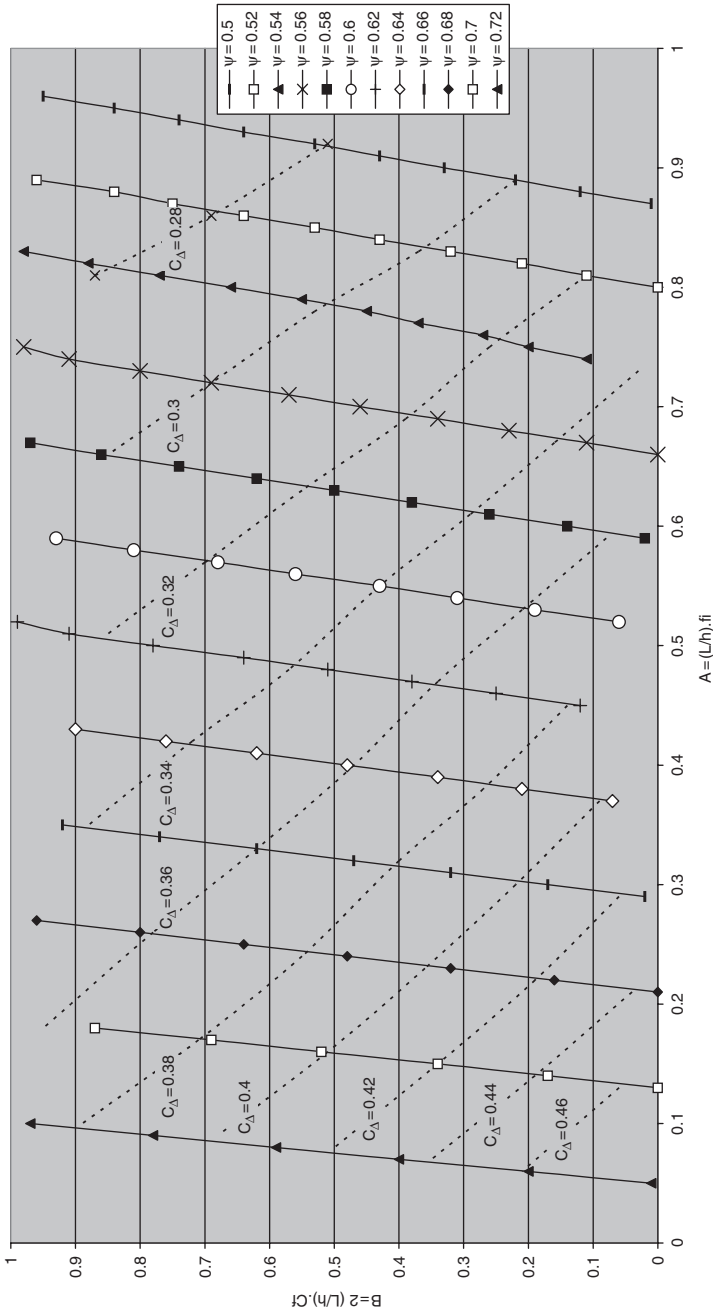


Figure 3. Couples (A, B) solutions, and isovalues of C_Δ satisfying the condition: $C_{a,\Delta} = C_{b,\Delta}$.

opening when A and B are known, or to estimate A and B in experiments where velocity and neutral plane position are observed. Then, the two nondimensional numbers C_Δ and ψ can be determined. For example, taking $A=B=0.1$ one finds the values $C_\Delta=0.46$ and $\psi=0.7$. It may be noted that the $C_\Delta=0.50$ is the highest possible value in Figure 3, which is then the terminal velocity for Phase 2 for frictionless flow. How much C_Δ is below 0.5 can therefore be considered a tool to measure the influence of bottom friction and turbulent shear stress in the interface between the inflowing and outflowing liquids.

Discussion of the Analytical Results

The equations leave one with implicit expressions for the depths of fluid 2 (the inflow), the adverse pressure at the wave head, and finally the inflow velocity. To complete the calculation, the length of the gravity wave L must be known. In Phase 2, this is $L=V_2.t$ where t is the elapsed time, but as the wave has acquired some length as Phase 2 starts, estimating L can be more complicated.

Friction is not very important for Phase 2 waves but plays a part. Pedersen [13] has investigated many results and come up with the formula for the interfacial friction factor f_i (Equation (23)), which is based on nine experimental series in a laboratory and four field study series by various researchers. The results show a great scatter, especially the experimental series. This is natural, as the velocity formulas clearly show that when they are used to calculate the friction factor, only a small deviation in y_2 creates a large deviation in the friction factor. In the same way, a small acceleration force will render a large deviation in the friction factor, but by using Pedersen's Figure (7.2), one finds that 0.01 is a fair estimate of f_i for clearly subcritical flows. In near-critical flows ($F_\Delta \leq 1$) the momentum exchange by increased entrainment can change this friction factor, as discussed in [13].

Phase 3: The Retarding Wave

When the L/h ratio grows large enough the friction term will dominate C_Δ , which becomes smaller and smaller, whatever the value of ψ is. At the same time, turbulent mixing and entrainment will change the density on both sides of the interface. In these processes, the entrainment velocity should be taken into account, but that depends on the Bulk Flux Richardson's number [13]. Such gravity waves

have to be very long and they are therefore very difficult to reproduce in the laboratory. In short compartments, the wave will hit the back wall and get reflected before Phase 3 starts. Therefore, the interest in Phase 3 waves from a fire protection engineering viewpoint is debatable. In situations leading to backdraft, it is more likely that the gravity wave will hit the opposite wall and be reflected from it before going into Phase 3. Therefore, one will not consider the analytical treatment of Phase 3 waves at this point.

COMPARISON WITH EXPERIMENTAL VALUES

Here one shall compare the theoretical results to three experiments. Two apply to the confined case and one to the unconfined case.

Experiments of Fleischman and McGrattan [1] (confined)

They conducted salt water experiments in their backdraft study and simulated the flow with a large eddy simulation turbulence model in a compartment [1]. This article gives a remarkable qualitative observation of the gravity wave, as well as detailed quantitative results on the propagation time of the wave and velocity field in the compartment, with a good agreement between salt water experiments and CFD simulations. The following experimental values for Δ and t^* are taken from Figure 5 in [1]. The velocities are then calculated using Equation (5) in [1] (L is here the total length of the compartment, t travel time across) $t = t^*L/\sqrt{\Delta gh}$, and $V_{ex} = L/t$.

From this, one has $C_{\Delta} = 1/t^* = 0.43$ with two significant digits. By using Figure 3, one gets ψ between 0.67 and 0.72. This result may be accurate enough, but if one has the friction data (not published in [1]), the complete theory of Phase 2 flow analytical results can be used to analytically determine ψ and C_{Δ} by using Equation (27). When one assumes $C_f = 0.003$, $f_i = 0.013$, one gets $A = 0.225$, $B = 0.107$, $\psi = 0.68$, and $C_{\Delta} = 0.43$.

Table 1 shows the experimental and analytical values for the terminal velocity.

Table 1 and Figure 4 show a very good agreement between experimental and analytical results, even if the terminal velocity has been calculated by only considering Phase 2. This shows that Phase 1 is very short and can consequently be neglected in the determination of the terminal velocity.

Table 1. Theory compared to Fleischmann and McGrattan results.

Fleishmann and McGrattan - Experiments				Theory Phase 2
Δ	t^*	t (s)	V_{ex} (m/s)	V_{an} (m/s)
0.01	2.3	5.69	0.053	0.052
0.018	2.2	4.06	0.074	0.070
0.04	2.25	2.78	0.108	0.104
0.07	2.3	2.15	0.140	0.137
0.1	2.2	1.72	0.174	0.164

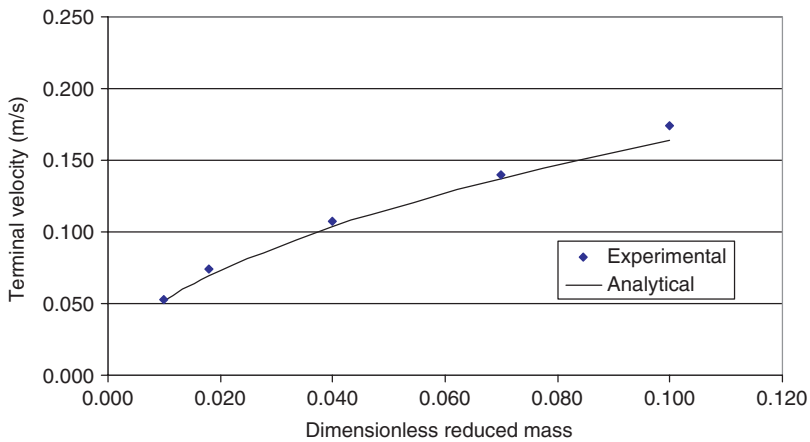


Figure 4. Terminal velocity versus Δ for experiments and analytical theory.

Experiments of Weng et al. [8] (confined)

In these experiments, one series is performed with a full opening. All the v^* results (terminal velocity in [8]) are $v^* = 0.49\text{--}0.50$. This terminal velocity is calculated the same way as C_Δ (Equation (27)) except that Weng et al. use the lighter fluid as reference density. Consequently, the v^* results are 2–5% higher than the C_Δ for the values reported in Table 1 in [8]. They would be $C_\Delta = 0.46\text{--}0.48$, or about 5% higher than the v^* values. However the agreement is very good.

Experiments of Moghtaderi [15] (unconfined)

Moghtaderi carried out experimental studies of the structure of gravity currents using a laser Doppler velocity meter. Experiments were

done in both adiabatic and isothermal conditions. The isothermal boundary conditions showed a three-dimensional turbulence, whereas adiabatic showed a more two-dimensional behavior. The turbulence was found to be highly heterogeneous and its distribution was governed by the location of large eddies, so one uses the adiabatic condition where this extra turbulence is not present. In these experiments, there is an unconfined (open channel) wave. The measured head velocity is $V_2 = 0.1 \text{ m/s}$, $\Delta = 0.048$ giving $C_\Delta = 0.42$ and the reported $L/h \cong 0.8/0.12 = 6.7$. From Table 1 in [15], the Reynolds number of the wave can be estimated as $Re_{e,L} = Vh/\nu \approx 8880$. As the L/h value is rather low [13], one uses Equation (24) for C_f .

$$C_f = \frac{1.3}{\sqrt{Re_{e,L}}} = \frac{1.3}{\sqrt{Re(L/h)}} = \frac{1.3}{\sqrt{8880 \cdot 6.7}} = 0.005.$$

Giving $B = 0.034$, Figure 3 shows $\psi = 0.66$. This results in $y_{2,0} = 0.08$ and compares well to Figure 9 in [15]. Then $A = 0.3$ is found by giving $f_i = 0.04$, considerably lower than the value of 0.1. Here one has a higher A and a lower f_i than in Fleischmann and McGrattan's experiments [1], just as one should have according to the appendix.

APPLICATIONS

Both physical and numerical experiments need to be carefully designed. A study of Figure 3 shows that C_Δ varies between 0.3 and 0.45 depending on A and B . Experiments with L/h ratios from 5 to 10 as is common in large buildings may be difficult to perform in a laboratory. This may be helped by making the floor rough to increase C_f in order to bring laboratory A and B up to prototype values.

Example 1

A reception hall is 25 m deep and 3 m high. At one end is a fireplace, and one wants to know the eventual travel time of the gravity wave to the fire place and measure it in a salt water experiment in a compartment in the scale $\lambda_h = 10$ in height and $\lambda_L = 15$ in length. Prototype C_f is estimated at 0.05 including furniture and decorations. What C_f for the model is needed?

$C_{f,m}/C_{f,p} = (Re_{L,p}/Re_{L,m})^{1/2} = (V_p/V_m)^{1/2} (L_{c,p}/L_{c,m})^{1/2} (\nu_m/\nu_p)^{1/2} = (\lambda_h \Delta_p / \Delta_m)^{1/4} \lambda_h^{1/2} (\nu_m/\nu_p)^{1/2} = (\Delta_p / \Delta_m)^{1/4}$ 1.8 3.9 0.26 = approximately 3–4. (here the subscripts m and p stand for the model and the prototype, respectively).

This applies if one builds a scaled model of the hall with all furniture and decorations. This will increase model A and B and bring up too low C_{Δ} results, and time travel results may be 20% too low. One must find a way to reduce model $C_{f,m}$ to $\approx 25\%$ of prototype $C_{f,p}$.

Example 2

A 40 m long corridor, 2.8 m high, is filled with hot gas with density 75% of air. It becomes extremely flammable when mixed with air. A glow has been detected at the far end. A deflagration travel time of 4 s can be added to the gravity wave travel time. Firemen can open the door and run for cover in 40s. Is it enough to escape the fireball? C_f is estimated 0.003.

$$L/h = 17.9, B = 0.1, A = 0.22 \Rightarrow C_{\Delta} = 0.43. t = 50 / (0.43 (0.25 \cdot 9.82 \cdot 2.8)^{1/2}) = 44 \text{ s.}$$

That should be OK! Even when not counting the deflagration travel time, which is reassuring. Nevertheless, a CFD analysis should be recommended.

DISCUSSION OF THE PHYSICS OF THE EXPERIMENTS

Experimental Results

The analytical values from Figure 4 are generally in good agreement with the experimental data. Taking Phase 1 into account improves the agreement a little, showing that friction terms must be interpreted carefully when the length/height (L/h) ratio is low. This is because of the Phase 1 time necessary for the accelerating wave to reach the terminal velocity value and the fact that Phase 1 is dominated by inertial forces rather than friction. The friction developed at the end of Phase 1 is quite high, but has little effect because of how small the L/h ratio is, it increases with the increasing L/h ratio of the wave, and can be estimated to be the dominating force when L/h reaches about 40. This is very close to the entrance length in pipes, or the length it takes for the boundary layer to reach the middle in a smooth pipe.

In Moghtaderi's experiments [15], one has a Phase 2 wave with L/h ratio significantly larger than in the unconfined experiments, but still too small to dominate the flow or bring it close to Phase 3. The consequences are that friction factors are high in the low L/h ratio experiments but diminish quickly. They are already up to 0.3 in Moghtaderi's experiment ($L/h = 6.7$) from about 0.1 in the other experiments.

In Phase 2 gravity flow, no appreciable mixing is produced. Entrainment is high at the beginning, but it decreases quickly, so when the compartment is fully open, a short gravity wave transports more or less clean air to the ignition point. When the air wave comes flowing through a narrow door or a window, one has a situation where the size of the opening determines the flow into the room through the formation of critical velocities in the opening. In this situation one has a gravity wave with a constant flow, but such waves are a little different from the purely translatory wave treated here. Another difference is that the plume into the compartment can easily cause appreciable forced mixing if it hits the floor from a considerable height. Then the initial mixture in the wave can have a Froude number different from the inflow.

CFD Calculations of Gravity Waves

Fleischmann and McGrattan's [1] CFD flow pictures are very interesting as they show a beginning vortex entrainment, which is generated inside the grid. Vortex entrainment and cusp entrainment exist in practice, and are discussed by Pedersen [13] (Figure 6.2). The vortices in [1] are however far too great and they cannot be seen in the actual experimental figures. The explanation of this discrepancy is twofold, first vorticity stretching is prohibited in 2D simulations, and second stable stratification slows down the mixing process. Mixing across a density stratification interface by action of turbulence creates potential energy that is taken out of the turbulent energy that otherwise would be dissipated. Turbulent dissipation is present in the sub-grid model only. The model may have to be modified to include this recycling of turbulent energy back into potential energy by action of turbulence, in order to represent the interface processes correctly. Figure 4.2.6 in Pedersen [13] explains this modification in a quantitative manner. Bournet et al. [16] calculate a plunging density current by using a $k-\varepsilon$ model where buoyancy is included in the macroscale model as well as in the sub-grid model, by including a term function dependent on the Prandtl number. They produce a convincing relation between entrainment and Richardson's number showing the characteristic sharp decline of entrainment with increasing stability (higher Ri). But they use a very special grid and special calculation procedures in order to preserve numerical stability. Kassem et al. [17] go a similar way with the same problem, and include the strain rate in the sub-grid model. They also produce convincing results, even for negative buoyancy. Comparing Fleischmann and McGrattan's simulation to Bournet and Kassem's

leave an unsolved question: should the potential energy gain be included in the sub-grid model in order to simulate gravity waves in backdraft simulations?

CONCLUSIONS

The gravity wave that feeds fresh air to closed compartments can be calculated using the equations of stratified flow given in the review papers by Pedersen [13]. Three flow phases can be identified, accelerating flow (Phase 1), translatory wave (Phase 2), and retarding flow (Phase 3).

The basic physical model for the unsteady motion of the gravity wave in Phase 2 is the translatory wave model. The wave progresses with constant velocity driven by the pressure gradient of the sloping interface. Such gravity waves on a horizontal bottom in a zero pressure environment do have the form of a parabola. In the mild adverse pressure gradient that drives the outflow, the parabolic form is assumed to be preserved without any loss of generality. The unknowns are basically the wave velocity, the wave's depth, and the pressure gradient driving the outflow. To calculate these quantities, there are three equations:

- (a) The depth integrated energy equation for the upper layer.
- (b) The momentum equation for both layers.
- (c) The momentum equation for the lower layer.

The velocity of this wave is governed by the densimetric Froude number of the wave, based on total fluid depth. With small friction, this Froude number turns out to be close to 0.44 in three different experiments, giving the entrance depth of the gravity wave up to 70% of the total depth.

The velocity of the wave and the thickness of the gravity wave in the entrance of the box can be found using Figure 3, provided that the interfacial and bottom friction is known. For short gravity waves, when interfacial and bottom friction are still small and the flow is in transition from Phase 1 to Phase 2, a dimensionless velocity C_Δ around 0.45 and a wave height ratio ψ (Equations (26) and (27)) around 0.72 are found.

A review of recent CFD calculations of stratified flows show a tendency to improve the sub-grid turbulence models by including terms that recycle a part of the turbulent energy production back into potential energy. This helps to reproduce the effect of the increasing stability of the stratification observed in nature on the entrainment. So far, it is unclear whether these improvements are necessary or not to

cope with the gravity wave in numerical backdraft simulations as frictional effects are not very important in low L/h waves. At least Fleischmann and McGrattan produce simulation results for a gravity wave on the borderline between Phase 1 and Phase 2 that, apart from large interface vortices, look convincing. Their results that fall within the formulas for both Phase 1 and Phase 2 are presented here.

Finally, It may be concluded that the method presented here gives reliable results for Phase 2 flows, and can be valuable in estimating gravity wave velocities and air carrying capacity. Scientists planning model tests and CFD simulations get a valuable advance knowledge of their problem when using this method. It also shows that fire safety experts can utilize research done inside the fluid mechanic community for the benefit of their own science.

NOMENCLATURE

- A = dimensionless coefficient. $A=(L/h)f_i$
 B = dimensionless coefficients. $B=2(L/h)C_f$
 C_f = bottom friction factor
 C_Δ = non-dimensional wave velocity
 D = depth
 f = friction factor
 f_i = interfacial friction factor
 F_Δ = densimetric Froude number
 g = acceleration of gravity
 g' = reduced acceleration of gravity
 h = height of the compartment (confined case) or total depth (unconfined case)
 I = energy gradient
 ℓ = length of the closed pathline
 L_c = length of the compartment
 L = longitudinal length of the wave
 P = pressure
 q = discharge per unit width
 q_1 = flow rate of hot fluid
 q_2 = flow rate of cold fluid
 R_e = Reynolds number
 R_{eL} = Reynolds number based on boundary layer length
 Ri = Richardson number
 S = coordinates in flow direction
 t = elapsed time after compartment opening

- t_a = acceleration time
 t^* = characteristic time
 U = velocity of the entrained fluid
 U_i = minimum velocity of the flow
 U_m = maximum velocity of the flow
 V = velocity of the gravity wave
 V_{av} = average velocity during the acceleration phase
 V_E = entrainment velocity
 V_{ex} = velocity values from experiments
 V_{max} = maximum velocity, at the end of the acceleration phase
 V_n = flow velocity at point n
 V_x = horizontal component of velocity
 V_y = vertical component of velocity
 V_1 = velocity of the hot fluid layer
 V_2 = velocity of the cold layer
 v^* = terminal velocity
 x = horizontal coordinates
 y = vertical coordinates
 y_c = critical depth
 y_L = total depth in front of the gravity wave
 y_n = vertical coordinates of point n
 y_1 = thickness of the hot fluid layer
 y_2 = thickness of the cold layer
 $y_{1,n}$ = thickness of the hot layer at point n
 $y_{2,n}$ = thickness of the cold layer at point n
 z = elevation
 δ = boundary layer thickness
 Δ = dimensionless reduced mass. $\Delta = (\rho - \rho_R)/\rho_R$
 λ = compartment scale factor for prototype
 λ_h = compartment scale factor (height)
 λ_L = compartment scale factor (length)
 ν = kinematic viscosity of the flow
 ξ = horizontal position inside the gravity wave
 ρ = fluid density
 ρ_R = density of the reference fluid
 ρ_1 = density of the hot fluid
 ρ_2 = density of the cold fluid
 τ = combined interfacial and bottom shear stress
 τ_i = interfacial shear stress
 τ_b = bottom shear stress
 ϕ = velocity potential function
 ψ = dimensionless gravity current thickness on depth ratio. $\psi = y_{2,n}/h$

APPENDIX 1: HYDRODYNAMICS OF STRATIFIED FLOWS

Here the general theory of stratified flows developed by Pedersen [13] is followed. We start by showing a simple case of non-miscible flow, then develop the theory leading to the flow chart on Figure 2, and introduce the effect of mixing later on stationary dense bottom currents.

A one-dimensional flow of heavy fluid along the bottom of a basin of light fluid of density ρ_R is considered. One can study the effect of a local hump by applying Bernoulli's equation along a streamline from A to B (see Figure A1):

$$\rho_R g D + \Delta \rho_R g y_A + \frac{1}{2} \rho_R (1 + \Delta) V_A^2 = \rho_R g D + \Delta \rho_R g y_B + \frac{1}{2} \rho_R (1 + \Delta) V_B^2. \quad (A1)$$

By using Boussinesq's approximation, one can neglect the difference between ρ_R and $\rho_R(1 + \Delta)$ except in the buoyancy term. One obtains, after simplification:

$$y_A + \frac{V_A^2}{2\Delta g} = y_B + \frac{V_B^2}{2\Delta g}. \quad (A2)$$

$$y_A + \frac{V_A^2}{2g'} = y_B + \frac{V_B^2}{2g'}. \quad (A3)$$

This shows that by using $g' = \Delta g$, all the well-known open channel flow equations can be reproduced. The dimensionless number:

$$F_\Delta = \frac{V}{\sqrt{g'y}} = \frac{V}{\sqrt{\Delta g y}} \quad (A4)$$

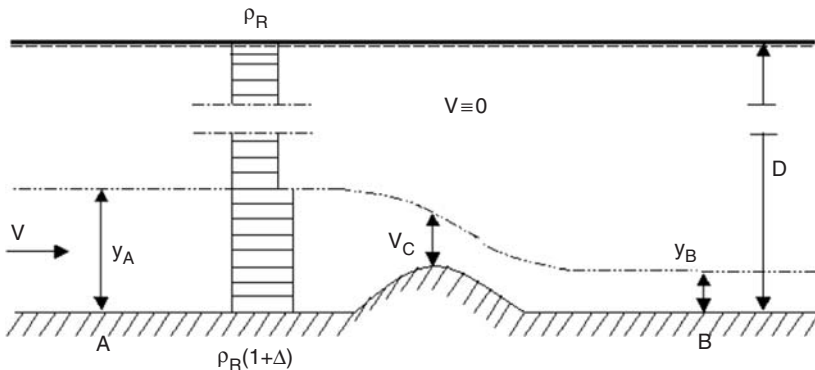


Figure A1. Schematic control volumes in a two layer zone model.

is called the densimetric Froude number and it characterizes the flow. All the well-known phenomena and relations applicable in open channel flow can be directly transferred to the dense bottom currents of the immiscible fluids using it. We just have to treat the current as if the acceleration of gravity were reduced to Δg . Then, specific energy and critical velocity arise when the Froude number is equal to one.

The Stationary Salt Water Wedge

This is an estuarine process, which has been much studied in laboratory testing and field observations. References to works by hundreds of researchers are in [13]. The light fresh water from a river floats on the more dense salt water of the sea (Figure A2). The density difference maintains a discharge in the upper fresh layer, and a circulation in the lower salt layer. This is very similar to the unsteady translatory wave used in many salt water tests in backdraft studies. In the interface, there is a shear stress:

$$\tau_i = \frac{f_i}{2} \rho (U_m - U_i)^2 = \frac{f_i}{2} \rho V^2 \tag{A5}$$

where f_i is the friction factor at the interface. The shear stress at the interface is balanced by the longitudinal pressure gradient in the lower fluid. One then has the differential equation for open channel flow. The depth integrated energy equation for the upper layer is:

$$I = -\frac{d}{dS} \left[y_2 + y_1 + \frac{V^2}{2g} \right]. \tag{A6}$$

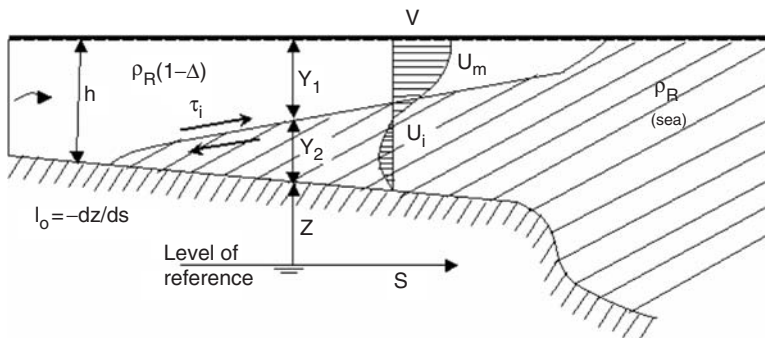


Figure A2. Stationary salt water wedge (highly distorted scale).

The depth integrated momentum equation allows one to write:

$$\tau_i = \rho_R(1 - \Delta)gy_1I \approx \rho_Rgy_1I. \quad (\text{A7})$$

APPENDIX 2: UNSTEADY TRANSLATORY GRAVITY WAVE ON A FLAT BOTTOM.

(a) No mixing

The wave starts when the compartment door is opened. In practice this will cause some initial pressure disturbance and a vortex formation in the compartment, which do not seem to be included in CFD simulations. The wave progresses with more or less constant velocity V (Figure 2), so the velocity of the fluid will also be V . Then the continuity Equation (12) allows the solution:

$$q = yV \quad y = y(\xi) \quad \xi = x - Vt$$

when V is constant energy loss is equal to surface slope. With friction proportional to the velocity squared and f_i representing the friction factor, the momentum equation gives:

$$\text{Momentum: } \frac{\partial y}{\partial \xi} = -I = -f_i \frac{V^2}{2gy}. \quad (\text{A8})$$

This equation integrates to:

$$\text{Wave form: } y^2 = f_i \frac{V^2}{\Delta g} (L - x) \quad (\text{A9})$$

The friction factor f is in two parts as before, bottom friction C_f and interfacial friction f_i that for small F_Δ can be estimated using Equation (23). $L = V \cdot t$ is the length of the wave from the opening. If y_0 corresponds to y in $x = 0$, the following wave form can be used instead of Equation (A9):

$$y^2 = y_0^2 \left(\frac{1 - x}{L} \right).$$

This is the most elementary form of a translatory wave. More complete forms can be for example found in Stoker [12].

(b) With mixing

No literature about mixing in translatory wave can be found, therefore the only possible way to estimate mixing effect is to use data for steady state (constant q) results. Phase 2 translatory waves are quasi-steady (V is constant) and in equilibrium with flow resistance, so effects of mixing should be similar. In CFD calculation this is the only data that the sub grid model, controlling local mixing, can be built on.

We have ([13] Equation (4.2.3))

$$\frac{\partial}{\partial x} \left(\frac{1}{2} \Delta \rho g y^2 + \rho V^2 y \right) + \rho V_E U + \tau_b + \tau_i = 0. \quad (\text{A10})$$

V_E is the entrainment velocity and U the velocity of the entrained fluid, that would essentially be proportional to the velocity of the upper fluid, that again is close to V . According to [13], V_E/V for high densimetric Froude numbers is of the order of magnitude 0.1 for buoyant plumes ([13] Equation (4.2.9)) and in dense bottom currents (13 Figure 6.6 and Equation (6.14)). These estimates by Pedersen are based on an immense number of laboratory data (see [13] Figures 7.1 and 7.2).

Judging from this, we would have three flow resistance terms, bottom friction, interfacial friction and entrainment resistance, all proportional to ρV^2 : Adding all up, the flow resistance in the mixing case should be

$$f_i \frac{1}{2} \rho V^2 = \left(\frac{V_E}{V} + C_f + f_i \right) \frac{1}{2} \rho V^2. \quad (\text{A11})$$

C_f and f_i are estimated using Equations (23) and (24), the friction factors are both an order of magnitude less than 0.1. In the mixing case, we therefore have $f_i \approx 0.1$.

The Phase 2 flow will start out with great mixing and a densimetric Froude number of 0.7–1.0 (Equation (4)). Judging from [13] Figure 6.6 when the velocity diminishes and Phase 2 turns into Phase 3, V_E/V quickly reduces and approaches the f_i and C_f values, but at the same time, L/h increases so A and B will most likely not diminish.

It should also be noted that mixing will increase the volume of the wave. The continuity equation only counts the dense liquid flow, ([13] chapter 4.1), so the neutral plane ($V=0$) will be higher. The total flow in the gravity wave will be the dense fluid plus entrained fluid.

$$q_t = q(x) + V_E x$$

Great care must therefore be taken when extending the Figure 3 results to Phase 3 flows. This can produce reliable results but cannot be generally recommended.

REFERENCES

1. Fleischmann, C.M. and McGrattan, K.B. (1999). Numerical and Experimental Gravity Currents Related to Backdrafts, *Fire Safety Journal*, **33**(1): 21–34.
2. Gojkovic, D., Initial Backdraft Experiments, Report 3121, Department of Fire Safety Engineering, Lund University, Sweden, 2001.
3. Weng, W.G. and Fan, W.C. (2002). Experimental Study on the Mitigation of Backdraft in Compartment Fires with Water Mist, *Journal of Fire Sciences*, **20**(4): 259–278, DOI: 10.1177/073490402762574721.
4. Zhou, F. and Wang, D. (2005). Backdraft in Descensionally Ventilated Mine Fire, *Journal of Fire Sciences*, **23**(3): 261–271. DOI: 10.1177/0734904105047915.
5. Fahy, R.F. and LeBlanc, P.R. (2006). Fire-fighters Fatalities in the United States – 2005. Fire Analysis and Research Division, National Fire Protection Association.
6. Weng, W.G. and Fan, W.C. (2003). Critical Condition of Backdraft in Compartment Fires: A Reduced Scale Experimental Study, *Journal of Loss Prevention in the Process Industries*, **16**(1): 19–26.
7. Fleischman, C.M., Pagni, P.J. and Williamson, R.B. (1994). Salt Water Modeling of Fire Compartment Gravity Currents. Fire Safety Science, In: *Proceedings of the Fourth International Symposium*, pp. 253–264; June 13–17, Ottawa, Ontario, Canada.
8. Weng, W.G., Fan, W.C., Qin, J. and Yang, L.Z. (2002). Study on Salt Water Modeling of Gravity Currents Prior to Backdrafts using Flow Visualization and Digital Particle Image Velocimetry, *Experiments in Fluids*, **33**(3): 398–404. DOI 10.1007/s00348-002-0448-1.
9. Weng, W.G. and Fan, W.C. (2004). Nonlinear Analysis of the Backdraft Phenomenon in Room Fires, *Fire Safety Journal*, **39**(6): 447–464.
10. Yanga, R., Weng, W.G., Fan, W.C. and Wang, Y.S. (2005). Subgrid Scale Laminar Flamelet Model for Partially Premixed Combustion and its Application to Backdraft Simulation, *Fire Safety Journal*, **40**(2): 81–98.
11. Eliasson, J., Kjaran, S.P., Holm, S.L., Gudmunsson, M.T. and Larsen, G. (2007). Large Hazardous Floods as Translatory Waves, *Environmental Modeling and Software*, **22**(10): 1392–1399.
12. Stoker, J.J. (1957). *Water Waves. The Mathematical Theory with Applications*, Interscience Publishers, London.
13. Pedersen, F.B. (1986). *Environmental Hydraulics: Stratified Flows*, Springer-Verlag Editions, Berlin, Heidelberg.
14. Olson, R.M. and Wright, S.J. (1990). *Essentials of Engineering Fluid Mechanics*, Fifth Edition, Harper and Row Publishers, New York.

15. Moghtaderi, B. (2004). Application of Laser Doppler Velocimetry (LVD) to Study the Structure of Gravity Currents under Fire Conditions, *Experimental Thermal & Fluid Science*, **28**: 843–852.
16. Bournet, P.E., Bartus, D., Tassin, B. and Vinçon-Leite, B. (1999). Numerical Investigation of Plunging Density Current, *Journal of Hydraulic Engineering*, **125**(6): 584–594.
17. Kassem, A., Imran, J. and Khan, J.A. (2003). Three Dimensional Modeling of Negatively Buoyant Flow in Diverging Channels, *Journal of Hydraulic Engineering*, **129**(12): 936–947.

BIOGRAPHIES

Jónas Eliásson

Jónas Eliásson graduated with a degree in Civil Engineering from DTH in 1962 and a pg.Lic.techn from the same school in 1973. He worked as an engineer in fluid mechanics with several Icelandic institutes and companies from 1964–1970 and Assistant Professor with DTH from 1970–1974. He was named professor of Fluid Dynamics, Hydrology and related subjects with the Department of Civil Engineering of the Faculty of Engineering and Science in 1973 and now works as such at the Department of Civil and Environmental Engineering at the Faculty of Engineering of the University of Iceland.

Georges Guigay

Georges Guigay studied at the Joseph Fourier University in Grenoble, France, where he gained a BSc degree in Mechanical Engineering in 1996 and a MSc degree in Numerical Simulation in 1998, specializing in Computational Fluid Dynamics. He has since been working as a researcher and a consulting engineer both in France and Iceland. In 2004, he joined a PhD program at the University of Iceland. His research focuses on underventilated fires and smoke gas explosions, such as backdraft.

Dr. Björn Karlsson

Dr. Björn Karlsson is born in Reykjavik 10th April 1959. He graduated in Civil Engineering (Hons) from Heriot-Watt University, Edinburgh 1986, acquired his Licentiate from the Department of Fire Safety Engineering at Lund University, Sweden in 1989 and received a PhD degree from the same department in 1992. He worked as Associate

Professor at the department from 1993 to 2001, was a Visiting Professor at the University of Maryland 1996, and became Fire Marshal and General Director of the state run Iceland Fire Authority, Reykjavik, Iceland in 2001.

Björn has written a number of books and articles in the field of fire safety, one of his best known works is the textbook “Enclosure Fire Dynamics”, published by CRC Press and coauthored by Professor James Quintiere at the Dept. of Fire Protection Engineering at the University of Maryland. He has given a large number of presentations at international seminars in Europe, USA, Canada, Japan, China and Australia. He sits on the board of the International Association for Fire Safety Science (IAFSS, www.iafss.org), is the Chairman of the IAFSS Education subcommittee, is on the editorial board of Fire Technology and on the editorial board of the International Journal on Engineering Performance-Based Fire Codes.

Björn is the vice-Chairman of the Icelandic Association of Chartered Engineers, Chairman of the Heating and Venting Association and the Secretary of the Association of Directors- General in Iceland. He is an Associate Professor at the Department of Environmental and Civil Engineering at the University of Iceland.